PHOTONICS Research

In situ instant generation of an ultrabroadband near-infrared emission center in bismuth-doped borosilicate glasses via a femtosecond laser

Liping Wang,[1] Jiangkun Cao,[1] Yao Lu,[2] Xiaoman Li,[3] Shanhui Xu,[1] Qinyuan Zhang,[1] Zhongmin Yang,[1] and Mingying Peng[1,*]

[1]State Key Laboratory of Luminescent Materials and Devices, Guangdong Engineering Technology Research and Development Center of Special Optical Fiber Materials and Devices, Guangdong Provincial Key Laboratory of Fiber Laser Materials and Applied Techniques, School of Materials Science and Engineering, South China University of Technology, Guangzhou 510641, China
[2]Department of Orthopedics, Zhujiang Hospital, Southern Medical University, Guangzhou 510282, China
[3]School of Physics and Physical Engineering, Shandong Provincial Key Laboratory of Laser Polarization and Information Technology, Qufu Normal University, Qufu 273165, China
*Corresponding author: pengmingying@scut.edu.cn

Received 20 August 2018; revised 9 January 2019; accepted 12 January 2019; posted 15 January 2019 (Doc. ID 342665); published 21 February 2019

Bismuth (Bi)-doped photonic materials, which exhibit broadband near-infrared (NIR) luminescence (1000–1600 nm), are evolving into interesting gain media. However, the traditional methods have shown their limitations in enhancing Bi NIR emission, especially in the microregion. Consequently, the typical NIR emission has seldom been achieved in Bi-doped waveguides, which highly restricts the application of Bi-activated materials. Here, superbroadband Bi NIR emission is induced *in situ* instantly in the grating region by a femtosecond (fs) laser inside borosilicate glasses. A series of structural and spectroscopic characterizations are summoned to probe the generation mechanism. And we show how this novel NIR emission in the grating region can be enhanced significantly and erased reversibly. Furthermore, we successfully demonstrate Bi-activated optical waveguides. These results present new insights into Bi-doped materials and push the development of broadband waveguide amplification.

https://doi.org/10.1364/PRJ.7.000300

1. INTRODUCTION

Integrated photonic circuits, which depend on miniaturization, flexibility, and combining multiple component designs, exhibit substantial applications in telecommunication, sensing, and monitoring [1–5]. Enormous efforts in recent years have been made to achieve optical amplification on planar optical waveguides for the demand of optical transmission [6,7]. Typically, four-wave mixing and self-phase modulation are normally used to broaden the amplification bandwidth on silicon waveguides [8]. However, highly precise signal matching is essential and difficult to realize, which evokes more difficulties in signal modulation and sophisticated optical design.

As an emerging fabrication technique, femtosecond (fs) laser microprocessing, with the unique advantages of ultrafast response time, high precision, and favorable flexibility, has been considered as a simple and effective way to fabricate optical waveguide amplifiers [3]. Up to now, via the fs laser writing technique, excellent optical waveguide amplifiers have been demonstrated, such as erbium-doped waveguide amplifiers [9] and ytterbium-doped $Y_3Al_5O_{12}$ crystals [7]. However, the current waveguide amplifiers, which are normally activated by rare-earth ions, suffer from narrow bandwidth. The bandwidth of most optical amplifiers doped with rare-earth ions is less than 50 nm. The amplification signals are restrained in the C (1525–1565 nm) and L (1565–1605 nm) bands, which hampers the full usage of low loss window, especially for the second transmission window. Due to the forbidden f–f transitions between the inner shell 4f orbits of rare-earth ions, the near-infrared (NIR) emission of rare-earth ions is highly insensitive to the local glass structure. It is almost impossible to further extend the bandwidth of rare-earth-doped optical waveguides via fs irradiation. Therefore, it is essential and of great significance to activate optical waveguides with broadband NIR emission via fs microprocessing, especially covering the whole optical transmission window.

Bismuth (Bi) ions within bulk glasses and fibers can exhibit ultrabroadband NIR luminescence, which spans the whole optical communication window from 900 to 1600 nm [10–12]. And Bi-functionalized optical amplification has been

demonstrated in Bi-doped fibers. Thus, Bi ions could activate an optical waveguide with broadband NIR emission so as to realize the amplification in the whole NIR region. As far as we know, when Bi ions are doped or diffused into the host, Bi NIR active ions are easily converted into other Bi species, such as Bi metals, Bi^{3+}, and Bi^{2+}. Bi NIR emission thus decreases and even quenches completely [13,14]. Therefore, much effort has been devoted to realizing effective and broad Bi NIR emission. So far, various methods have been employed to enhance their NIR emission, including modulating the coordination of aluminum, applying reducing atmosphere, and high-energy irradiation [15–17]. However, the current strategies are limited to the body of bulk glasses or fibers. All these cannot space-selectively precipitate Bi NIR emission centers and enhance their emission inside transparent glasses. As a result, the challenge still remains for the fabrication of Bi-doped waveguides due to the lack of modulating strategy of Bi NIR emission in the microregion, which surely restricts the application of Bi-doped materials in microdevices.

Here, by fs laser direct writing, we successfully activate gratings inside Bi-doped borosilicate glasses, which present superbroadband NIR emission (full width at half-maximum, FWHM > 300 nm). Bi NIR emission centers are generated instantly in the grating region and stabilized at ambient temperature. This unique NIR emission ranging from 1000 to 1600 nm is significantly enhanced by 2 orders compared to that of the sample without irradiation. And it can be erased flexibly through appropriate thermal stimulation. The generation mechanism is well discussed to offer insight on Bi-activated photonic materials. Moreover, we also present a strengthening strategy by the photoionization effect. Finally, this ultrabroad NIR emission is demonstrated successfully in Bi-activated waveguides. This work is a proof of concept, and we believe the quality of waveguides can be further improved by optimizing the profile of the refractive index and the emission distribution of the cross section. The results are of great importance for further studies on Bi-doped materials for potential applications in integrated optical devices.

2. EXPERIMENT

A. Sample Preparation

Borosilicate glasses exhibiting a large glass formation region, high third-order nonlinear optical susceptibility, and optical transmission have been employed widely in photonic materials [18,19]. Molar composition of borosilicate glasses $(80\text{-}x\text{-}y)B_2O_3 \cdot xPbO \cdot ySiO_2 \cdot 18Bi_2O_3 \cdot 2Sb_2O_3$ ($x = 0$, 5, 15, 20, 25, 35, 45) were prepared by the conventional melt-quenching method in air atmosphere, which were coded as BxPS ($x = 0$, 5, 15, 20, 25, 35, 45), respectively. The molar ratio of B_2O_3:SiO_2 is 4:1. B_2O_3, SiO_2, PbO, Bi_2O_3, and Sb_2O_3 (99.9% purity, Sigma-Aldrich) were employed as raw materials. 60 g batches were mixed homogeneously in an agate mortar, and then melted in alumina crucibles at 1200°C for 40 min. The melts were subsequently poured onto a stainless steel plate and pressed with another plate immediately. The samples were cut to dimensions of 10 mm × 10 mm × 1.5 mm and polished optically for subsequent microprocessing and measurements. All samples are transparent and colorless.

B. Characterizations

A commercial Ti:sapphire regenerative amplifier (Legend Elite Series, Coherent Inc.) system, emitting pulses with central wavelength of 800 nm, 50 fs duration, and 1 kHz repetition rate, was employed as the laser source. The laser pulse was focused on 300 μm beneath the surface of glass samples using a microscope objective (Nikon, 50×, numerical aperture 0.80). Microstructure gratings with 5 mm × 5 mm were fabricated under 6.0 μJ per laser pulse energy at a speed of 10 μm/s along the x axis, perpendicular to the laser propagation axis (z axis). 25 μm of line interval and 15 μm of width were determined to ensure that the grating region was connected closely in plates. The Fs laser pulse energy was adjusted by a continuous light attenuator and calibrated by a power meter (Serial No. M00256500, Thorlabs Inc.). The diffraction patterns were obtained by an He–Ne laser at 632.8 nm.

Absorption spectra were measured with a Perkin Elmer Lambda 900 UV/VIS/NIR spectrophotometer in a spectral range from 200 to 3200 nm. NIR emission spectra were taken on a Zolix Omni λ3007 spectrometer (Zolix Instruments, Inc., Beijing, China) equipped with an InGaAs photodetector and a SR830 Stanford Research lock-in amplifier. A continuous wave 808 nm GaAlAs semiconductor laser diode (LD) was used as the excitation source. The laser is output in parallel. Visible luminescence spectra were measured on an Edinburgh FLS 920 spectrofluorometer equipped with a liquid nitrogen cooled photomultiplier (Hamamatsu R5509-72). Elements mapping distributions were performed on an electron probe microanalyzer (EPMA-1600, Shimadzu). The valence state of Bi was measured by X-ray photoelectron spectroscopy (XPS) using a Kratos Axis Ultra DLD spectrometer equipped with a focused monochromatic Al K_α X-ray beam (1486.6 eV, 5 mA × 10 kV, $\sim 5 \times 10^{-9}$ Torr), and the binding energy was calibrated to the C 1s peak at 284.6 eV. The diffuse reflectance spectra (DRS) were collected on a Cary 5000 UV–VIS–NIR spectrophotometer. The 532 nm laser with ∼5 mW of output power is generated by the second-harmonic of a 1064 Nd:YAG laser source. It was used to measure Raman spectra in the spectral range from 10 to 4000 cm^{-1} on a Renishaw InVia spectrometer. Fourier transform infrared (FTIR) spectra were recorded on a Bruker Vector 33 spectrometer by homogeneously dispersing samples in KBr pellets. ^{11}B MAS nuclear magnetic resonance (NMR) spectra were measured using Bruker AVANCE III HD 400 instruments. NIR emission of the waveguide was detected by a fiber optical spectrometer (QE65pro, Ocean Optics). The multimode fiber pigtailed to the Ocean Optics spectrometer was 1.2 m long with a numerical aperture of 0.22. The refractive index was recorded on a prism coupling apparatus (Metricon Model 2010). Waveguide transmission losses were measured over propagation distances of 0.5–2.5 cm at 1310 nm with the cutback technique. The input light was coupled to the sample by aligning the fibers directly with the waveguide. The output light was coupled to the photodetector through a focusing microscope objective, which collected most of the outgoing light. All measurements were performed at room temperature.

3. RESULTS AND DISCUSSION

A. *In situ* Instant Generation of Bi NIR Emission Centers under fs Laser Irradiation

Gratings with a large size of 5 mm × 5 mm were prepared inside glass for convenience to measure the absorption spectra. The top of Fig. 1(a) shows the optical microscope image of gratings under 6.0 μJ of pulse energy. All samples are transparent and colorless before fs laser irradiation. After fs laser irradiation, the grating region of the samples turns directly reddish brown, as shown in the bottom of Fig. 1(a). The reddish brown deepens gradually as pulse energy increases from 2.0 to 8.0 μJ. An obvious absorption peak at 512 nm is observed in the region [see Fig. 1(b)], which is from typical absorption of Bi NIR emission centers [20]. Absorption coefficients increase from 0.95 to 5.64 cm^{-1} with laser pulse energy from 2.0 to 8.0 μJ. The data are fitted well by an exponential equation with a correlation ($R = 0.993$), as shown in the blue curve of Fig. 1(d). Clearly, Bi NIR emission centers are induced in the grating region after fs laser irradiation.

Furthermore, we measured the emission spectra of the grating region with different laser pulse energies upon 808 nm excitation. Bi NIR emissions are hardly observed before fs laser irradiation [see the blue curve of Fig. 1(c)]. Ultrabroadband Bi NIR emissions are enhanced significantly in the range from 1000 to 1600 nm after fs laser irradiation. As laser pulse energy increases from 2.0 to 8.0 μJ, Bi NIR luminescence is enhanced by 15, 36, 76, and 174 times, respectively, compared to before fs laser irradiation [see Figs. 1(c) and 1(d)]. The intensity of Bi NIR emission also exhibits exponential growth along with increasing laser pulse energy. Therefore, ultrabroadband Bi NIR emission could be induced under fs laser irradiation and enhanced by increasing the laser pulse energy.

To clarify the generation mechanism of Bi NIR emission centers, we first measured the relative distribution of B, O, and Bi elements around a laser-focused point [see Fig. 2(a)]. From the electron probe microanalysis (EPMA) mapping, one can see that the relative content of the Bi element has no obvious change. This result indicates that the increase of Bi NIR emission centers cannot be attributed to the migration of the Bi element at the laser-focused point. However, O and B elements migrate in opposite directions. The imperfect beam profile may be responsible for the asymmetry redistribution of the B and O elements. Because of the heat accumulation effect of the high repetition rate, the temperatures increase drastically to 2000 K at the laser-focused point [21,22]. The imperfect beam profile of the laser may lead to the asymmetric distribution of temperature around the focused region, thus causing the nonuniform migration of elements. The O element involves a higher diffusion coefficient than the B element [23]; thus, it moves easily out of the high temperature region. The B element is forced to migrate to the low O region to eliminate the concentration gradient, thus exhibiting high content in the low O region. This thus leads to the opposite distribution of B and O around the laser-focused point. The glass network formers are mainly constituted by B and O atoms. The dramatic redistribution of B and O indicates the transformation of the glass network structure under fs laser irradiation.

Further, we explored the variation of the glass network structure around the laser-focused region by micro-Raman spectra. The Raman spectrum of the B0PS sample without irradiation

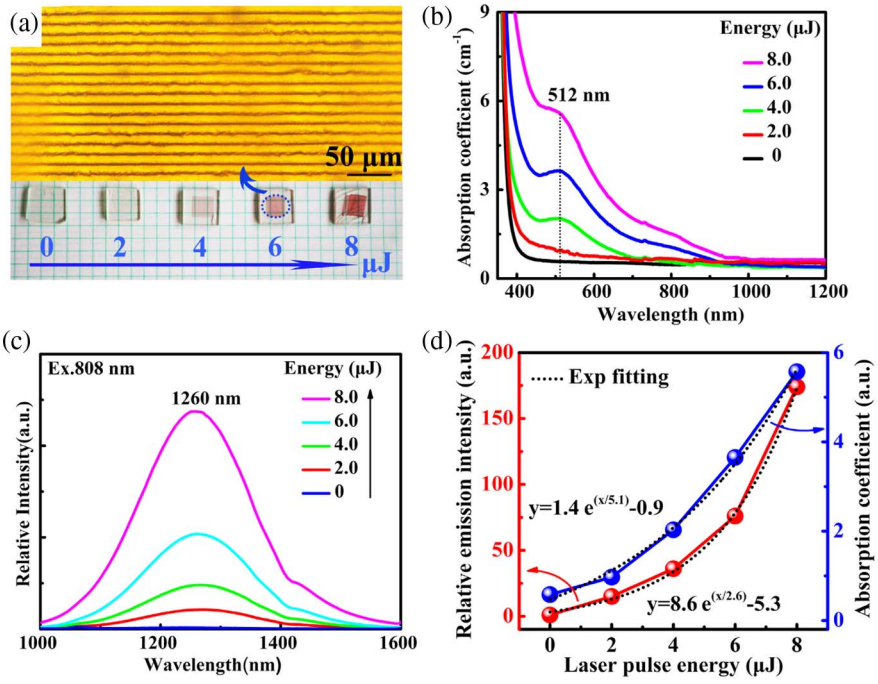

Fig. 1. Absorption and NIR emission of B0PS sample after fs laser irradiation. (a) Optical microscope image of grating under 6.0 μJ of fs laser pulse energy, and photographs of B0PS sample irradiated under different pulse energy (0–8.0 μJ, as labeled); (b) UV/VIS/NIR absorption and (c) NIR emission spectra ($\lambda_{ex} = 808$ nm) of the B0PS sample with increasing fs laser pulse energy; (d) dependence of Bi NIR emission intensity (red curve) and absorption coefficients (blue curve) on the pulse energy of the fs laser.

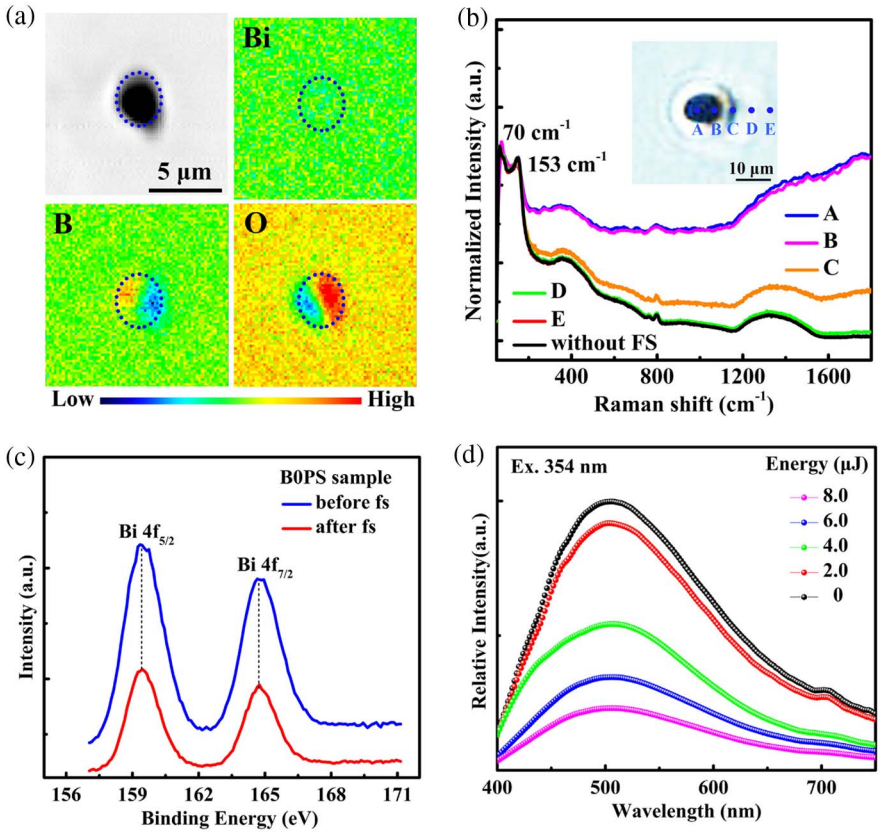

Fig. 2. Element migration, micro-Raman spectra, and visible fluorescence spectra in the fs laser-focused region. (a) Backscattering electron image and element distribution showing the relative concentrations of O, B, and Bi around the fs laser focal point; (b) micro-Raman spectra of the fs laser-focused region with different positions under 2.0 μJ of pulse energy. The Raman spectrum of the B0PS sample without fs irradiation is added for comparison (black curve). (c) XPS profiles at the Bi 4f core level of the B0PS sample before and after fs laser irradiation; (d) visible fluorescence spectra of the B0PS sample upon 354 nm excitation with laser pulse energy from 0 to 8.0 μJ.

was added for comparison (black curve). The low-frequency region exhibits two sharp bands at 70 and 153 cm^{-1} [see the black curve in Fig. 2(b)]. The peak at 70 cm^{-1} is clearly related to the acoustic Raman modes of heavy metal Bi cations as Miller *et al.* [24] have demonstrated in a series of glasses containing different metal oxides. And the peak at 153 cm^{-1} is definitely attributed to the vibration of Bi^{3+} cations as [BiO_6] octahedral units. It has been demonstrated that the characteristic peak matches α-Bi_2O_3 well, which indicates that the valence state of Bi is +3. [25,26]. The peak at 366 cm^{-1} and its shoulder peak at 650 cm^{-1} in the middle-frequency region are assigned to the stretching vibration of Bi-O-Bi and Bi-O- in the distorted [BiO_6] units, respectively [27]. In the high-frequency range, the broadbands at 820–1165 cm^{-1} and 1165–1565 cm^{-1} are characteristic of stretching vibration of B-O-B from [BO_4] tetrahedral and planar [BO_3] triangles, respectively [28,29]. After fs laser irradiation, these characteristic bands can also be observed in the irradiation region. The sharp Raman peaks at 153 cm^{-1} from Bi^{3+} cations become weaker gradually as the distance decreases from the surroundings (points B, C, D, and E) to the center (point A), which indicates the decrease of Bi^{3+} ions of the irradiation region. From margin E to center A, the intensity of stretching vibration of Bi-O-Bi at 366 cm^{-1} decreases gradually while the signal from Bi-O- at 650 cm^{-1} increases. This means that bridge oxygen bonds of Bi-O-Bi are broken into nonbridge oxygen bonds under ultrastrong fs laser peak power density. The increase of nonbridge oxygen bonds may cause the glass network structure of the irradiation region to become looser. Meanwhile, the stretching vibration of B-O-B from tetrahedral [BO_4] at 820–1165 cm^{-1} decreases gradually from the surrounding points to the center. In contrast, the broadband at 1165–1565 cm^{-1} from triangles [BO_3] increases consistently. These results indicate the transformation of glass network formers from [BO_4] to [BO_3] units under fs laser irradiation. As we know, planar BO_3 triangles exhibit a lower cross-linked network than tetrahedral [BO_4]. Thus, one could infer that the glass network structure is depolymerized under fs laser irradiation. The looser glass network structure cannot efficiently isolate Bi NIR emission centers. This will greatly increase the probability of nonradiation transition. In this case, Bi NIR emission becomes weaker than that of the sample before fs laser irradiation. However, Bi NIR luminescence of the irradiation region is enhanced significantly. Therefore, the generation of Bi NIR centers could not be ascribed to the evolution of the glass network structure and element migration under fs irradiation.

Previously, photoreduction of active ions has occurred via fs laser irradiation. For example, Sm^{3+} and Eu^{3+} were

converted into Sm^{2+} and Eu^{2+}, respectively, under ultrastrong fs laser pulse energy [30,31]. Here, we believe that the generation of Bi NIR centers could also be ascribed to the valence change of Bi ions under fs laser irradiation. We have attempted to measure the contents of Bi NIR emission centers by either X-ray photoelectron spectroscopy (XPS) or extended X-ray absorption fine structure (EXAFS). Two characteristic peaks are observed at 159.6 and 164.6 eV in the XPS profiles, respectively, which are consistent with the reported 4f spectrum of α-Bi_2O_3 [see Fig. 2(c)] [32]. They are ascribed to $4f_{7/2}$ and $4f_{5/2}$ of Bi^{3+}, respectively. However, this change cannot be distinguished before and after fs laser irradiation. This may be because traditional valence detection techniques, such as XPS and EXAFS, are not sensitive to Bi species, which cannot detect the exact concentration of Bi NIR emission centers and confirm their types. Besides, the concentration of Bi NIR emission centers is very low in the irradiated region, which is below the limits of detection of XPS. Therefore, the change of valence of Bi ions cannot be detected by the XPS profiles. Over the past few decades, various types of Bi NIR emission centers have been proposed [33–43]. On the basis of thorough works, low-valence Bi species, e.g., Bi^{+} or Bi^{0}, have been considered widely as NIR emission centers. Besides, it has been confirmed that visible luminescence was attributed to Bi^{3+} or Bi^{2+} ions [44]. In this work, the absorption and emission spectra were employed to detect the change of Bi species before and after fs laser irradiation because these measurement methods are more sensitive to Bi ions. As fs laser pulse energy increases from 2.0 to 8.0 μJ, visible luminescence from Bi^{3+} at 504 nm decreases sharply under 354 nm excitation [see Fig. 2(d)], but Bi NIR emission increases, as shown in Fig. 1(c). On the basis of these results, we considered that the enhancement of Bi NIR emission may be attributed to the valence change from high-valence Bi^{3+} to low-valence Bi NIR active ions, such as Bi^{0} or Bi^{+}, under fs laser irradiation.

The reduction of Bi ions may be due to avalanche ionization under ultrastrong fs laser power density. Avalanche ionization is a common nonlinear optical phenomenon of the interaction of fs lasers with transparent material, and it has been proved previously by world-famous scientists, such as Mazur, Hirao, and Kazansky [45–47]. In this work, when the laser pulse energy is 2.0 μJ and the diameter of the laser-focused point is 20 μm, the fs laser peak power density reaches 1.3×10^{13} W/cm^2 at the laser-focused point. At such ultrastrong power density, electrons absorb energy from multiple photons and pass from the valence band to the conduction band. When the stimulated electron energy is strong enough, impact ionization occurs and triggers electrons of other ions to the conduction band. Avalanche ionization will thus be achieved, and free electrons of the conduction band will exhibit an exponential increase. Here, we consider that avalanche ionization may occur under fs laser irradiation and thus cause the change of the valence of Bi ions by the photoreduction reaction as follows:

$$Bi^{n+} + xe^{-} \xrightarrow{fs} Bi^{(n-x)+}. \quad (1)$$

As the photoreduction reaction proceeds to the right direction, high-valence Bi ions, such as Bi^{3+} and Bi^{2+}, are converted to low valence after fs laser irradiation. Low-valence Bi species increase greatly, and high-valence Bi^{3+} ions decrease. Bi NIR emission from low-valence Bi species is thus enhanced [see Fig. 1(c)], while visible luminescence decreases dramatically in the irradiation region [see Fig. 2(d)]. According to the multiphoton absorption equation,

$$P(I) = \sigma_k I^k, \quad (2)$$

where P is the probability of multiphoton absorption, σ_k is the multiphoton absorption cross section for the absorption of k photons, I is the laser peak intensity [48], and the probability of multiphoton absorption P increases exponentially with increasing laser intensity and photon number k. Correspondingly, the number of ionized free electrons increases exponentially with the laser intensity. According to reaction (1), Bi NIR emission centers increase with the increase of ionized free electrons. Thus, the absorption coefficient and Bi NIR emission increase exponentially with laser pulse peak intensity, as shown in Fig. 1(d).

B. Enhancing the Bi NIR Emission of the Grating Region

As explored above, ultrabroadband Bi NIR emission is induced in the fs laser irradiated region and enhanced by increasing the fs laser pulse energy. However, micro/nanocracks or voids may occur in the irradiation region as the fs laser pulse energy increases continually [49]. The occurrence of microcracks will hamper the Bi NIR emission of the grating region. Hence, we should seek another powerful strategy to enhance the Bi NIR luminescence of the grating region. According to the generation mechanism of Bi NIR emission centers, ionized free electrons can reduce Bi species from high valence to low valence under fs irradiation. Bi NIR luminescence is thus enhanced with the increase of low-valence Bi NIR centers. Therefore, we should stimulate the formation of more free electrons to enhance Bi NIR emission. As we all know, a Pb atom exhibits the same electronic configuration as a Bi^{+} ion. Under fs laser irradiation, the electron cloud of its outer orbits is easily ionized due to the large atom radius [50]. A large number of free electrons may be produced under fs laser irradiation. Besides, PbO exists as a glass network intermediator in a borosilicate glass system [51]. Previous studies have shown that Bi NIR luminescence can be enhanced by adding glass network intermediates [20]. Furthermore, Pb-doped glasses exhibit high optical transmission and superior nonlinear optical susceptibility and mechanical properties. They will efficiently avoid the occurrence of micro/nanocracks and voids under strong laser irradiation. For these reasons, different contents of PbO were added into the B0PS glass, which were coded as BxPS (x = 0, 5, 15, 20, 25, 35, 45, x% represents the molar fraction of PbO).

Before fs laser irradiation, absorption peaks cannot be observed for all BxPS samples (x = 0, 5, 15, 20, 25, 35, 45). This indicates the ultralow content of Bi NIR emission centers in the host materials. Correspondingly, Bi NIR emission is extremely weak under 808 nm excitation, as shown in Fig. 3(a). The emission increases gradually as PbO content increases from 0 to 20%, and reaches a maximum at 20%, then decreases. Bi NIR emission of B20PS (x = 20) is enhanced by 5 times relative to that of the B0PS sample without PbO. To reveal the enhancement mechanism, we explored the evolution

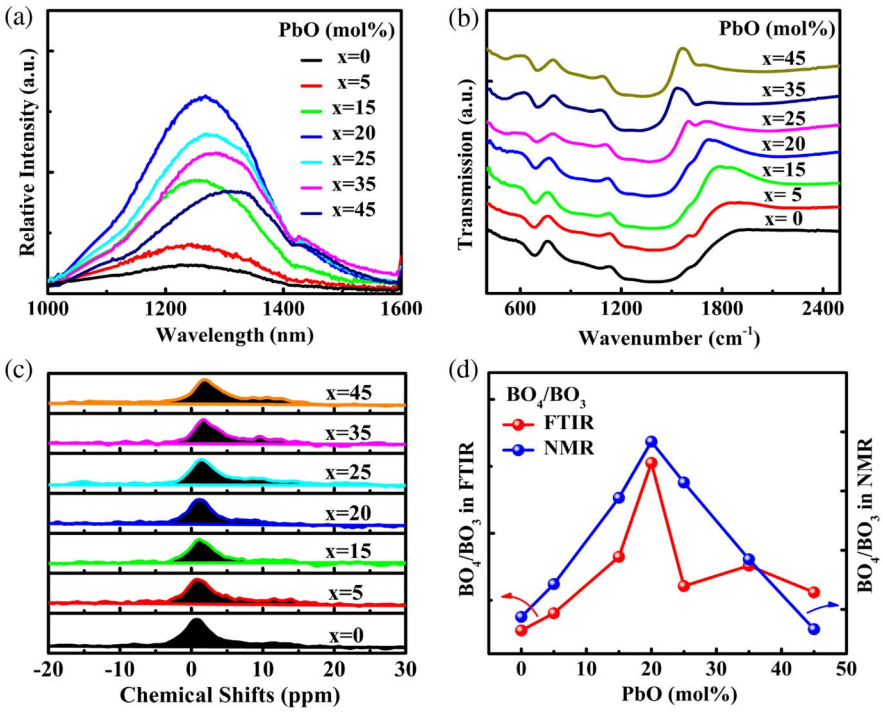

Fig. 3. NIR emission and structure analysis of BxPS glasses without fs laser irradiation. (a) Emission (λ_{ex} = 808 nm), (b) FTIR, and (c) ^{11}B MAS NMR spectra of BxPS glasses (x = 0, 5, 15, 20, 25, 35, 45) before fs laser irradiation; (d) relative ratio of $[BO_4]/[BO_3]$ in ^{11}B MAS NMR and FTIR spectra, respectively, as a function of PbO content.

of the glass network structure of BxPS glasses by FTIR spectra and ^{11}B NMR spectra. In the FTIR spectra, four broadbands are observed at ~491 cm^{-1}, ~690 cm^{-1}, 800–1200 cm^{-1}, and 1200–1500 cm^{-1}, respectively [see Fig. 3(b)]. The broadband at ~491 cm^{-1} is assigned to the deformation vibration of Pb-O from a $[PbO_4]$ tetrahedron [19]. At low PbO content (x = 0–20), the broadband from the $[PbO_4]$ tetrahedron was not obvious. As PbO content increases from 20% to 45%, the vibration intensity of the $[PbO_4]$ tetrahedron increases gradually. This indicates the formation of a $[PbO_4]$ tetrahedron at high PbO content (x = 20–45). The broadband at ~690 cm^{-1} results from the bending vibration of B-O-B from the $[BO_3]$ triangle. The vibration intensity becomes weaker with increasing PbO content from 0 to 20%, and then increases until PbO content of 45%. The other two broadbands at 800–1200 cm^{-1} and 1200–1500 cm^{-1} are attributed to the stretching vibration of B-O- of the $[BO_4]$ and $[BO_3]$ units, respectively [28]. PbO as a glass network intermediate will lead to the conversion of $[BO_4]$ and $[BO_3]$ [18]. We calculate the relative ratio of $[BO_4]/[BO_3]$ through the integral intensity [see Fig. 3(d)]. The relative ratio of $[BO_4]/[BO_3]$ increases gradually with increasing PbO content from 0 to 20%, reaches a maximum at 20%, and then decreases. In the NMR spectra, the peaks at ~0 and ~10^{-5} are considered a chemical shift from $[BO_4]$ and $[BO_3]$, respectively, as shown in Fig. 3(c) [18,29]. The relative ratio of $[BO_4]/[BO_3]$ presents the same trend [see Fig. 3(d)]. Therefore, the variation of Bi NIR luminescence properties may be due to the evolution of the glass network structure.

At low PbO content (x = 0–20), PbO acts as a glass network modifier. The oxygen atoms from PbO are coordinated preferentially to $[BO_3]$ units, causing the conversion of $[BO_3]$ into $[BO_4]$ units. The relative ratio of $[BO_4]/[BO_3]$ increases with the addition of PbO content, as shown in Fig. 3(d). The glass network structure is polymerized gradually with increasing PbO from 0 to 20% because the $[BO_4]$ tetrahedron involves a higher cross-linked network than $[BO_3]$ units. High network polymerization efficiently isolates Bi NIR emission centers. The probability of nonradiation transition decreases significantly. Bi NIR luminescence of BxPS glasses is thus enhanced below 20% [see Fig. 3(a)]. When PbO content is higher than 20%, PbO acts as a glass network former. A $[PbO_{4/2}]^{2-}$ tetrahedron forms gradually, as shown in Fig. 3(b). The relative ratio of $[BO_4]/[BO_3]$ decreases because glass network formers $[BO_4]$ are substituted preferentially for the $[PbO_4]$ tetrahedron. But $[PbO_{4/2}]^{2-}$ involves higher negative charges than $[BO_{4/2}]^{-}$. In order to maintain the electric neutrality of the glass network structure, excess positive charges are forced to oxidize low-valence Bi NIR centers into high-valence Bi species. As low-valence Bi NIR emission centers decrease, Bi NIR luminescence decreases gradually at high PbO content.

To obtain higher gain of Bi-activated waveguides, Bi NIR emission of waveguides should also be enhanced. Enhancing Bi NIR emission of the grating region means the enhancement of Bi-activated waveguides. Thus, we further explored the effect of the addition of PbO on Bi NIR emission of the grating region. The same grating structures were prepared inside BxPS glasses (x = 5, 15, 20, 25, 35, 45) under 6.0 μJ of laser pulse energy. For all samples, the grating region transformed instantly into reddish brown after fs irradiation. The reddish brown deepens gradually as PbO content increases, as shown in the inset of

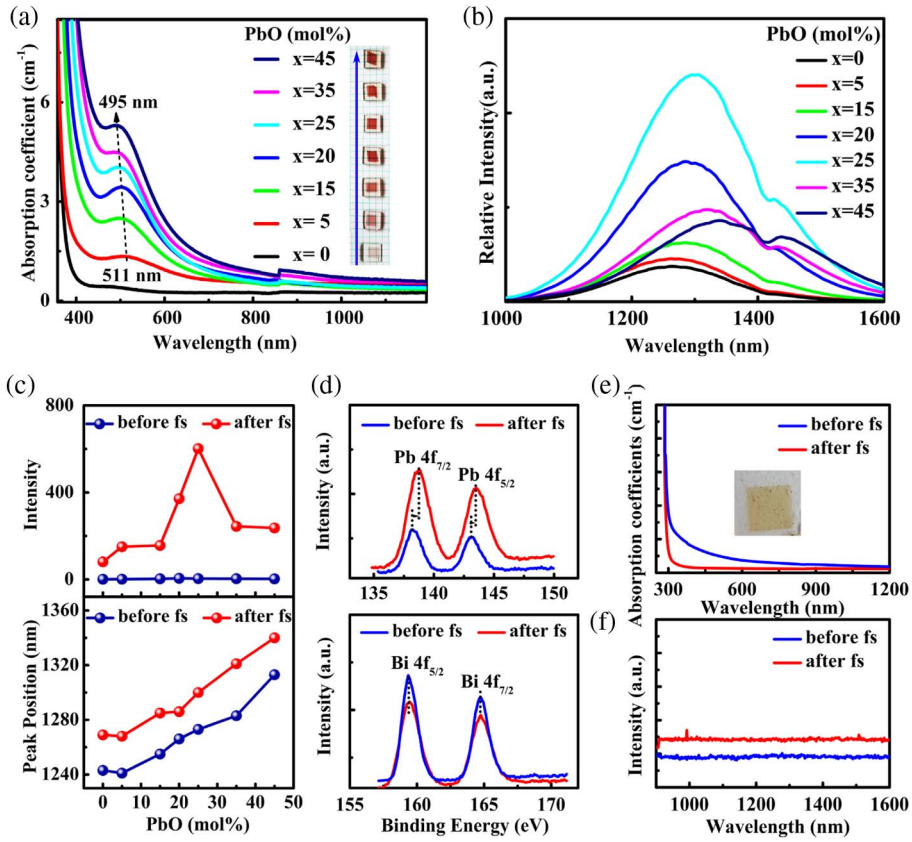

Fig. 4. Absorption, Bi NIR emission of B*x*PS glasses, and the sample $60B_2O_3$–$15SiO_2$–$23PbO$–$2Sb_2O_3$ without Bi_2O_3 before and after fs laser irradiation. (a) Absorption and (b) Bi NIR emission spectra ($\lambda_{ex} = 808$ nm) of the grating region of B*x*PS ($x = 0, 5, 15, 20, 25, 35, 45$) glasses. The inset in (a) shows photographs of the B*x*PS sample after fs laser irradiation. (c) The dependence of emission intensity and peak position on PbO content ($x = 0$–45); (d) XPS profiles at Pb and the Bi 4f core level of the B25PS sample before and after fs laser irradiation; (e) absorption and (f) emission spectra of the 60 B_2O_3–$15SiO_2$–$23PbO$–$2Sb_2O_3$ sample without Bi_2O_3 before and after fs laser irradiation.

Fig. 4(a). In the colored region, typical absorption peaks from Bi NIR centers are observed in all samples, as shown in Fig. 4(a). The jump at 860 nm is due to the switch of the grating. A holographic grating with 1440 lines per mm is used in the UV/VIS range from 185 to 860 nm. A grating with 360 lines per mm is employed in the NIR range from 860 to 3200 nm. The absorption coefficients of B*x*PS samples increase gradually, and the absorption peaks exhibit blueshift from 511 to 487 nm. Clearly, the addition of PbO induces more Bi NIR active ions under fs laser irradiation.

The Bi NIR emission of the grating region was measured under 808 nm excitation. As shown in Fig. 4(b), the broadband NIR emissions from 1000 to 1600 nm are presented in all the samples. For Pb-doped samples, where PbO content is 5%–45%, Bi NIR emissions are enhanced by 2 orders of magnitude relative to that before fs laser irradiation [see Figs. 4(b) and 4(c)]. For example, the emission of the B25PS sample is enhanced by 600 times after fs laser irradiation. Before fs laser irradiation, Bi NIR emission is enhanced only by 6.5 times with increasing PbO content from 0 to 25%, as shown in Fig. 3(a), which is due to the polymerization of the glass network structure, as shown in Figs. 3(b) and 3(c). After fs laser irradiation, Bi NIR emissions of all the glass samples are enhanced by 2 orders of magnitude relative to that before fs laser irradiation. Clearly, laser irradiation is more efficient in enhancing Bi NIR emission. The emission intensity increases gradually as PbO content increases from 0 to 25% and reaches a maximum at 25%, then decreases gradually as PbO content increases from 25% to 45%. The decrease in emission intensity should be attributed to concentration quenching at the high content of PbO because the absorption increases continually. The redshift should be due to the enhanced reabsorption, and the absorption spectra overlap with the emission spectra, as shown in Fig. 4(a). It also contributed perhaps to the enhancement of the local crystal field around Bi NIR active ions. It will lower the lowest excited levels.

To explore the enhancement mechanism, the chemical environment of Pb and Bi elements was measured by XPS before and after fs laser irradiation. As shown in Fig. 4(d), typical symmetric peaks are observed at 138.2 and 143.2 eV in the B25PS sample before fs laser irradiation, which are from Pb^{2+} with binding energies of $4f_{7/2}$ and $4f_{5/2}$, respectively [52]. These two binding energies increase simultaneously after fs laser irradiation [see Fig. 4(d)], indicating the decrease of average electron density around Pb atoms. But there is no shift to be observed in the binding energy of the Bi element for the B25PS sample [see Fig. 4(d)]. As described in Section 3.A, it may be because the measurement methods are not sensitive

to Bi NIR emission centers, and the content of Bi NIR emission centers is very low in the irradiated region. Therefore, the increase of electron density around Bi ions also cannot be observed directly by the XPS profiles. Electrons of the outer orbits on Pb atoms are ionized under ultrastrong laser pulse energy. Ionized electrons increase gradually with the addition of PbO. These released electrons will accelerate the reaction (1) to the right direction. Correspondingly, high-valence Bi ions are converted into low-valence Bi NIR emission centers [see Fig. 4(a)]. The valence change of Bi ions indicates the increase of the electron density after fs laser irradiation. The increase of Bi NIR emission centers thus leads to the enhancement of the Bi NIR emission of the grating region of B*x*PS samples ($x = 0, 5, 15, 20, 25, 35, 45$) after adding PbO.

Also, the enhancement may be attributed to the change of host glass materials after fs laser irradiation. To explore the effect of irradiation on the host glass materials, the sample $60B_2O_3$–$15SiO_2$–$23PbO$–$2Sb_2O_3$ without Bi_2O_3 was prepared under the same melting conditions. As shown in Figs. 4(e) and 4(f), no absorption peak and NIR emission can be observed before and after fs laser irradiation. The irradiation region turns from colorless into light yellow, which may be attributed to the valence change of lead ions from low valence to high valence via photoionization [see Fig. 4(d)]. Therefore, it also indicates that the addition of PbO provides more electrons to Bi ions, thus producing more Bi NIR emission centers.

C. Reversible Bi NIR Emission of the Grating Region

Utilizing the fs laser microprocessing technique, Bi NIR emission can be one-step-induced in the grating region and stabilized at ambient temperature. To achieve multiple manipulation of Bi NIR emission of the irradiation region, we endeavored to erase the Bi NIR emission of the grating region. This will provide a reference model for designing erasable Bi-doped waveguides. To our best knowledge, Bi NIR species easily experience valence change under high temperature [53,54]. Utilizing the sensitivity of Bi NIR active ions to thermal stimulation, we attempted to erase the Bi NIR emission of the irradiation region by annealing.

The B25PS sample with 25% of PbO and the B0PS sample without PbO were chosen to explore the effect of annealing on the Bi NIR luminescence of the grating region. First, the same gratings were fabricated inside the B25PS and B0PS samples under 6.0 μJ of laser pulse energy. Then the irradiated samples were annealed for 0, 5, 10, 20, 40, and 60 min, respectively. To our best knowledge, the glass network structure may change dramatically around a glass transition temperature of 463°C, which may lead to the change of the Bi NIR emission. To avoid the change of the glass structure, glass samples should be annealed below the glass transition temperature. Therefore, the annealed temperature was selected at 400°C. As the annealing time was prolonged, the reddish brown of the irradiated region degraded gradually, as shown in the inset of Fig. 5(b),

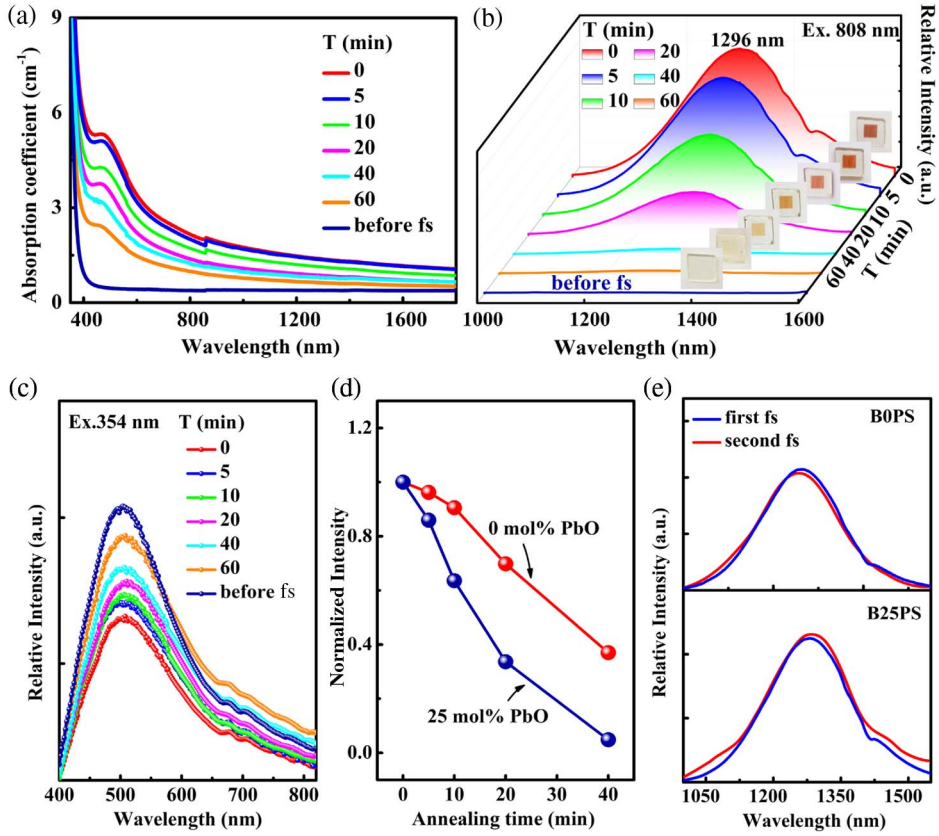

Fig. 5. Absorption, NIR emission, and visible luminescence of the B25PS irradiated sample after annealing. (a) Absorption, (b) NIR emission ($\lambda_{ex} = 808$ nm), and (c) visible fluorescence ($\lambda_{ex} = 354$ nm) of the irradiation region of the B25PS sample annealed at 400°C for 0, 5, 10, 20, 40, and 60 min, respectively. The inset in (b) shows the corresponding photographs of the B25PS sample. (d) The dependence of the Bi NIR emission intensity of the B0PS and B25PS samples on annealing time; (e) Bi NIR emission spectra of the B0PS and B25PS samples after first and second fs laser writing.

indicating the decrease of Bi NIR active ions. We further measured absorption spectra of the samples with different annealing times. The absorption coefficients decrease dramatically with increasing annealing time [see Fig. 5(a)]. Correspondingly, the Bi NIR emission of the B25PS sample decreases monotonically upon 808 nm excitation [see Fig. 5(b)]. And the Bi NIR emission of the B25PS sample exhibits a blueshift from 1296 to 1270 nm. When the annealing time is 60 min, the emission intensity reduces to that before fs laser irradiation, and the peak position shifts back the emission position of the sample before fs laser irradiation, as shown in Fig. 5(b). Similar variation was observed in the B0PS sample under the same annealing condition. Bi NIR emission can also be observed at other temperatures below glass transition temperatures. For example, when the B25PS sample is annealed at 300°C, the Bi NIR emission can also be erased with the disappearance of the reddish brown of the irradiation region.

Bi NIR emission can be rewritten in the grating region. Here, we rewrote the grating inside the B0PS and B25PS samples annealed for 60 min. The irradiation region and irradiation conditions are the same as that of the first irradiation. The emission intensity and peak exhibit faint variation compared to the first irradiation, as shown in Fig. 5(e). For the sample B25PS, the intensity of the Bi NIR emission increases barely after the second irradiation, and the peak shifts slightly from 1296 to 1298 nm. Clearly, the Bi NIR emission of the irradiation region can be erased and rewritten reversibly by annealing.

The visible luminescence of grating region was measured to explore the erasure mechanism. As shown in Fig. 5(c), the visible luminescence from Bi^{3+} is enhanced gradually under 354 nm excitation as the annealing time increases, indicating the increase of high-valence Bi^{3+} ions. As the annealing time increases, low-valence Bi NIR emission centers are oxidized gradually into high-valence Bi^{3+} via thermal relaxation. Low-valence Bi NIR active ions such as Bi^{0} and Bi^{+} decrease, but high-valence Bi^{3+} ions increase gradually. Correspondingly, Bi NIR emission becomes weaker, and the visible emission from Bi^{3+} ions increases gradually. Thus, the erasure of the Bi NIR emission is attributed to the valence change of Bi NIR active ions from low valence to high valence under thermal stimulation.

Further, we analyze the effect of PbO on the erasure rate. The degradation rate of the Bi NIR emission of the B25PS and B0PS samples was quantified. As shown in Fig. 5(d), the intensity of the Bi NIR emission decreases linearly with increasing annealing time. According to the slope of the fitted curves, the erasure rate of B25PS is accelerated by 28 times by adding 25% of PbO. As PbO is added into the glass system, the glass network former [BO_4] is substituted by [PbO_4] units, as explored above. [PbO_4] exhibits lower packing factors than the [BO_4] tetrahedron [18]. B25PS glass has a larger free volume than the B0PS sample without PbO. A larger free volume is beneficial to the oxidation of Bi NIR active ions. Thus, the erasure rate of Bi NIR emission can be accelerated by adding PbO.

D. Broadband Emission from Bi-Doped Waveguides

Finally, we selected a B25PS sample to demonstrate simply the fluorescence from Bi-activated waveguides. The change of refractive index was measured by the diffraction pattern [see Fig. 6(a)]. The first-order diffraction efficiency is 10% by the ratio of second-order diffraction intensity and incident light intensity. The change of refractive index is 4.7×10^{-4} by this equation:

$$\eta = (\pi \Delta n d/\lambda \cos\theta)^2, \tag{3}$$

where d is the thickness of the gratings, θ is the angle between the surface normal and the diffracted laser beam, and the laser wavelength λ is 632.8 nm [55]. We further measured the refractive index of the grating region of the B25PS sample with a prism coupler. The refractive index of the B25PS sample at 633 nm is 1.8389 and 1.8398 before and after fs laser irradiation, respectively. Therefore, the change of refractive index Δn is positive. It makes it possible to achieve Bi-activated waveguides. The waveguide was fabricated 300 μm below the glass surface. The pump light enters the sample from one side of the waveguide. Ultrabroadband NIR luminescence from the Bi-activated waveguide was detected at the other side of the waveguide by 3 W/cm^2 of 808 nm pumping. The broadband emission from the Bi-activated waveguide covers from 1000 to 1600 nm with an FWHM of 236 nm. Compared to waveguide samples, Bi NIR luminescence can hardly be observed, as shown in Fig. 6(b). Actually, the B25PS sample also exhibits NIR luminescence, which is very weak and can only be observed in the magnified spectra [see Fig. 6(b)]. This originates from the ultralow content of Bi NIR emission centers in the

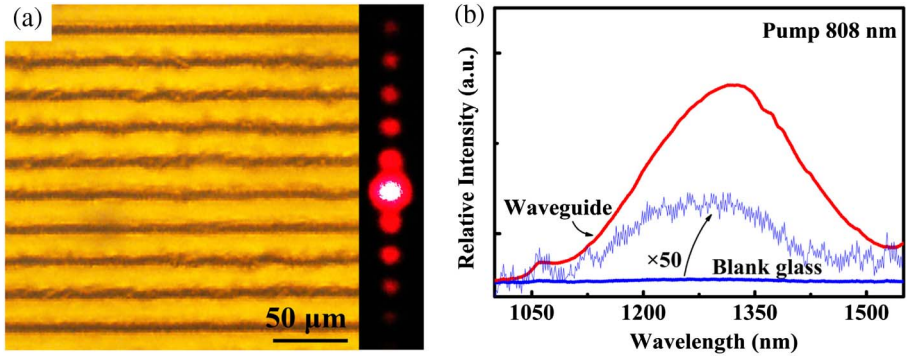

Fig. 6. Illustration of Bi-activated optical waveguide. (a) Optical microscope image of gratings inside the B25PS sample under 6.0 μJ laser pulse energy and the diffraction pattern of an He–Ne laser at 632.8 nm; (b) Bi NIR emission when pumping the waveguide under 808 nm irradiation (3 W/cm^2).

B25PS sample. Furthermore, we have measured the transmission loss of waveguides at 1310 nm using the cutback method, and its propagation loss was 0.68 dB/cm. The propagation loss of the waveguide written in the borosilicate glass is higher than that in pure silica, which is 0.12 dB/cm [56]. Currently, the work is only a proof of concept, and it can be further improved by the proper design of glass compositions and optimizations of other parameters for laser writing.

4. CONCLUSIONS

The key to extending the amplification bandwidth of a waveguide is to realize the modulation of novel active ions with ultrabroad NIR emission in the microregion. Here, via fs direct writing, we demonstrate the fabrication of Bi-functionalized gratings inside borosilicate glasses. The typical ultrabroadband Bi NIR luminescence is obtained instantly in the grating region and stabilizes permanently at ambient temperature. We discover that the generation of Bi NIR centers is due to the photoreduction reaction of Bi NIR active species from high-valence Bi^{3+} ions to low-valence under fs laser irradiation. Furthermore, Bi NIR emission of the grating region is enhanced significantly by 600 times through adding PbO after fs laser irradiation, offering a new way to enhance Bi NIR emission in a local region. Moreover, this novel emission can be erased by thermal treatment and rewritten by fs irradiation. As a proof of concept, we demonstrate the ultrabroadband Bi NIR emission from a waveguide under 808 nm pumping, indicating the potential applications in a Bi-activated waveguide amplifier. Although the quality and the refractive index change of the waveguide should be further improved, it provides guidance for realizing Bi-doped waveguide amplifiers with efficient gain in the future.

Funding. Natural Science Foundation of Guangdong Province (2018B030308009); National Natural Science Foundation of China (NSFC) (51672085); Program for Innovative Research Team in University of Ministry of Education of China (IRT_17R38); Ministry of Education of the People's Republic of China (MOE); Local Innovative Research Team Project of "Pearl River Talent Plan" (2017BT01X137); Fundamental Research Funds for the Central Universities.

REFERENCES

1. K. M. Davis, K. Miura, N. Sugimoto, and K. Hirao, "Writing waveguides in glass with a femtosecond laser," Opt. Lett. **21**, 1729–1731 (1996).
2. Q. Wang, E. T. F. Rogers, B. Gholipour, C. M. Wang, G. H. Yuan, J. H. Teng, and N. I. Zheludev, "Optically reconfigurable metasurfaces and photonic devices based on phase change materials," Nat. Photonics **10**, 60–65 (2016).
3. D. Z. Tan, K. N. Sharafudeen, Y. Z. Yue, and J. R. Qiu, "Femtosecond laser induced phenomena in transparent solid materials: fundamentals and applications," Prog. Mater. Sci. **76**, 154–228 (2016).
4. C. L. Sun, Y. Yu, G. Y. Chen, and X. L. Zhang, "Ultra-compact bent multimode silicon waveguide with ultralow inter-mode crosstalk," Opt. Lett. **42**, 3004–3007 (2017).
5. Y. Hayasaki, T. Sugimoto, A. Takita, and N. Nishida, "Variable holographic femtosecond laser processing by use of a spatial light modulator," Appl. Phys. Lett. **87**, 031101 (2005).
6. T. J. Wang, D. Zhao, M. L. Zhang, J. Yin, W. Y. Song, Z. X. Jia, X. B. Wang, G. S. Qin, W. P. Qin, F. Wang, and D. M. Zhang, "Optical waveguide amplifiers based on $NaYF_4$:Er^{3+}, Yb^{3+} NPs-PMMA covalent-linking nanocomposites," Opt. Mater. Express **5**, 469–478 (2015).
7. N. Jornod, V. J. Wittwer, C. Kränkel, D. Waldburger, U. Keller, T. Südmeyer, and T. Calmano, "High-power amplification of a femtosecond vertical external-cavity surface-emitting laser in an Yb:YAG waveguide," Opt. Express **25**, 16527–16533 (2017).
8. Y. Wu, B. C. Yao, Q. Y. Feng, X. L. Cao, X. Y. Zhou, Y. J. Rao, Y. Gong, W. L. Zhang, Z. G. Wang, Y. F. Chen, and K. S. Chiang, "Generation of cascaded four-wave-mixing with graphene-coated microfiber," Photon. Res. **3**, A64–A68 (2015).
9. G. D. Valle, R. Osellame, N. Chiodo, S. Taccheo, G. Cerullo, P. Laporta, A. Killi, U. Morgner, M. Lederer, and D. Kopf, "C-band waveguide amplifier produced by femtosecond laser writing," Opt. Express **13**, 5976–5982 (2005).
10. E. M. Dianov, "Bismuth-doped optical fibers: a challenging active medium for near-IR lasers and optical amplifiers," Light Sci. Appl. **1**, e12 (2012).
11. M. Y. Peng, J. R. Qiu, D. P. Chen, X. G. Meng, L. Y. Yang, X. W. Jiang, and C. S. Zhu, "Bismuth and aluminum codoped germanium oxide glasses for super-broadband optical amplification," Opt. Lett. **29**, 1998–2000 (2004).
12. B. B. Xu, J. H. Hao, Q. B. Guo, J. C. Wang, G. X. Bai, B. Fei, S. F. Zhou, and J. R. Qiu, "Ultrabroadband near-infrared luminescence and efficient energy transfer in Bi and Bi/Ho co-doped thin films," J. Mater. Chem. C **2**, 2482–2487 (2014).
13. L. P. Wang, N. J. Long, L. H. Li, Y. Lu, M. Li, J. K. Cao, Y. Zhang, Q. Y. Zhang, S. H. Xu, Z. M. Yang, C. B. Mao, and M. Y. Peng, "Multifunctional bismuth-doped bioglasses: combining bioactivity and photothermal response for bone tumor treatment and tissue repair," Light Sci. Appl. **7**, 1 (2018).
14. B. B. Xu, S. F. Zhou, M. J. Guan, D. Z. Tan, Y. Teng, J. J. Zhou, Z. J. Ma, Z. L. Hong, and J. R. Qiu, "Unusual luminescence quenching and reviving behavior of Bi-doped germanate glasses," Opt. Express **19**, 23436–23443 (2011).
15. W. Shen, J. Ren, S. Baccaro, A. Cemmi, and G. Chen, "Broadband infrared luminescence in γ-ray irradiated bismuth borosilicate glasses," Opt. Lett. **38**, 516–518 (2013).
16. A. Winterstein, S. Manning, H. E. Heidepriem, and L. Wondraczek, "Luminescence from bismuth-germanate glasses and its manipulation through oxidants," Opt. Mater. Express **2**, 1320–1328 (2012).
17. J. K. Cao, L. Y. Li, L. P. Wang, X. M. Li, Z. Y. Zhang, S. Xu, and M. Y. Peng, "Creating and stabilizing Bi NIR-emitting centers in low Bi content by topo-chemical reduction and tailoring local glass structure," J. Mater. Chem. C **6**, 5384–5390 (2018).
18. T. Taigo, J. Jin, U. Takashi, and Y. Toshinobu, "Structural study of PbO-B_2O_3 glasses by X-ray diffraction and ^{11}B MAS NMR techniques," J. Am. Ceram. Soc. **83**, 2543–2548 (2010).
19. B. Suresh, M. S. Reddy, A. S. S. Reddy, Y. Gandhi, V. R. Kumar, and N. Veeraiah, "Spectroscopic features of Ni^{2+} ion in PbO-Bi_2O_3-SiO_2 glass system," Spectrochim. Acta A **141**, 263–271 (2015).
20. M. Y. Peng, C. Wang, D. P. Chen, J. R. Qiu, X. W. Jiang, and C. S. Zhu, "Investigations on bismuth and aluminum co-doped germanium oxide glasses for ultra-broadband optical amplification," J. Non-Cryst. Solids **351**, 2388–2393 (2005).
21. F. F. Luo, B. Qian, G. Lin, J. Xu, Y. Liao, J. Song, H. Y. Sun, B. Zhu, J. R. Qiu, Q. Z. Zhao, and Z. Z. Xu, "Redistribution of elements in glass induced by a high-repetition-rate femtosecond laser," Opt. Express **18**, 6262–6269 (2010).
22. M. Shimizu, M. Sakakura, S. Kanehira, M. Nishi, Y. Shimotsuma, K. Hirao, and K. Miura, "Formation mechanism of element distribution in glass under femtosecond laser irradiation," Opt. Lett. **36**, 2161–2163 (2011).
23. G. Popovici, R. Wilson, T. Sung, M. Prelas, and S. Khasawinah, "Diffusion of boron, lithium, oxygen, hydrogen, and nitrogen in type IIa natural diamond," J. Appl. Phys. **77**, 5103–5106 (1995).
24. A. E. Miller, K. Nassau, K. B. Lyons, and M. E. Lines, "The intensity of Raman scattering in glasses containing heavy metal oxides," J. Non-Cryst. Solids **99**, 289–307 (1988).
25. L. Baia, R. Stefan, P. Jürgen, S. Simon, and W. Kiefer, "Vibrational spectroscopy of highly iron doped B_2O_3-Bi_2O_3 glass systems," J. Non-Cryst. Solids **324**, 109–117 (2003).

26. K. Trentelman, "A note on the characterization of bismuth black by Raman micro-spectroscopy," J. Raman Spectrosc. **40**, 585–589 (2009).
27. Y. P. Zhang, Y. X. Yang, Y. W. Ou, H. Wei, J. H. Zheng, and G. R. Chen, "Effect of Sb_2O_3 on thermal properties of glasses in Bi_2O_3-B_2O_3-SiO_2 system," J. Am. Ceram. Soc. **92**, 1881–1883 (2009).
28. L. Stoch and M. Środa, "Infrared spectroscopy in the investigation of oxide glasses structure," J. Mol. Struct. **511**, 77–84 (1999).
29. Y. D. Yiannopoulos, G. D. Chryssikos, and E. I. Kamitsos, "Structure and properties of alkaline earth borate glasses," Phys. Chem. Glasses **42**, 164–172 (2001).
30. D. Nishida, E. Yamade, M. Kusaba, T. Yatsuhashi, and N. Nakashima, "Reduction of Sm^{3+} to Sm^{2+} by an intense femtosecond laser pulse in solution," J. Phys. Chem. A **114**, 5648–5654 (2010).
31. J. R. Qiu, K. Kojima, K. Miura, T. Mitsuyu, and K. Hirao, "Infrared femtosecond laser pulse-induced permanent reduction of Eu^{3+} to Eu^{2+} in a fluorozirconate glass," Opt. Lett. **24**, 786–788 (1999).
32. J. Han, F. J. Pan, M. S. Molokeev, J. F. Dai, M. Y. Peng, W. J. Zhou, and J. Wang, "Redefinition of crystal structure and Bi^{3+} yellow luminescence with strong near-ultraviolet excitation in La_3BWO_9:Bi^{3+} phosphor for white light-emitting diodes," ACS Appl. Mater. Interfaces **10**, 13660–13668 (2018).
33. Y. Fujimoto and M. Nakatsuka, "Infrared luminescence from bismuth-doped silica glass," Jpn. J. Appl. Phys. **40**, L279–L281 (2001).
34. R. Quimby, R. Shubochkin, and T. Morse, "High quantum efficiency of near-infrared emission in bismuth doped AlGeP-silica fiber," Opt. Lett. **34**, 3181–3183 (2009).
35. J. J. Ren, J. R. Qiu, D. P. Chen, X. Hua, X. W. Jiang, and C. S. Zhu, "Luminescence properties of bismuth-doped lime silicate glasses," J. Alloys Compd. **463**, L5–L8 (2008).
36. J. Y. Zheng, M. Y. Peng, F. W. Kang, R. P. Cao, Z. J. Ma, G. P. Dong, J. R. Qiu, and S. H. Xu, "Broadband NIR luminescence from a new bismuth doped $Ba_2B_5O_9Cl$ crystal: evidence for the Bi^0 model," Opt. Express **20**, 22569–22578 (2012).
37. T. Murata and T. Mouri, "Matrix effect on absorption and infrared fluorescence properties of Bi ions in oxide glasses," J. Non-Cryst. Solids **353**, 2403–2407 (2007).
38. S. Khonthon, S. Morimoto, Y. Arai, and Y. Ohishi, "Redox equilibrium and NIR luminescence of Bi_2O_3-containing glasses," Opt. Mater. **31**, 1262–1268 (2009).
39. B. Denker, B. Galagan, V. Osiko, S. Sverchkov, and E. Dianov, "Luminescent properties of Bi-doped boro-alumino-phosphate glasses," Appl. Phys. B **87**, 135–137 (2007).
40. M. Y. Sharonov, A. B. Bykov, V. Petricevic, and R. R. Alfano, "Spectroscopic study of optical centers formed in Bi-, Pb-, Sb-, Sn-, Te-, and In-doped germanate glasses," Opt. Lett. **33**, 2131–2133 (2008).
41. E. M. Dianov, "Nature of Bi-related near IR active centers in glasses: state of the art and first reliable results," Laser Phys. Lett. **12**, 095106 (2015).
42. J. Y. Zheng, L. L. Tan, L. P. Wang, M. Y. Peng, and S. H. Xu, "Superbroad visible to NIR photoluminescence from Bi^+ evidenced in $Ba_2B_5O_9Cl$: Bi crystal," Opt. Express **24**, 2830–2835 (2016).
43. A. N. Romanov, A. A. Veber, Z. T. Fattakhova, D. N. Vtyurina, M. S. Kouznetsov, K. S. Zaramenskikh, I. S. Lisitsky, V. N. Korchak, V. B. Tsvetkov, and V. B. Sulimov, "Spectral properties and NIR photoluminescence of Bi^+ impurity in $CsCdCl_3$ ternary chloride," J. Lumin. **149**, 292–296 (2014).
44. J. Han, L. J. Li, M. Y. Peng, B. L. Huang, F. J. Pan, F. W. Kang, L. Y. Li, J. Wang, and B. F. Lei, "Toward Bi^{3+} red luminescence with no visible reabsorption through manageable energy interaction and crystal defect modulation in single Bi^{3+}-doped $ZnWO_4$ crystal," Chem. Mater. **29**, 8412–8424 (2017).
45. P. P. Pronko, P. A. VanRompay, C. Horvath, F. Loesel, T. Juhasz, X. Liu, and G. Mourou, "Avalanche ionization and dielectric breakdown in silicon with ultrafast laser pulses," Phys. Rev. B **58**, 2387–2390 (1998).
46. P. G. Kazansky, H. Inouye, T. Mitsuyu, K. Miura, J. R. Qiu, and K. Hirao, "Anomalous anisotropic light scattering in Ge-doped silica glass," Phys. Rev. Lett. **82**, 2199–2202 (1999).
47. R. G. Rafael and M. Eric, "Femtosecond laser micromachining in transparent materials," Nat. Photonics **2**, 219–225 (2008).
48. K. Yamanouchi, S. L. Chin, P. Agostini, and G. Ferrante, *Progress in Ultrafast Intense Laser Science I* (Springer, 2009), p. 241.
49. L. P. R. Ramirez, M. Heinrich, S. Richter, F. Dreisow, R. Keil, A. V. Korovin, U. Peschel, S. Nolte, and A. Tünnermann, "Tuning the structural properties of femtosecond-laser-induced nanogratings," Appl. Phys. A **100**, 1–6 (2010).
50. H. D. Zeng, G. R. Chen, J. R. Qiu, X. W. Jiang, C. S. Zhu, and F. X. Gan, "Effect of PbO on precipitation of laser-induced gold nanoparticles inside silicate glasses," J. Non-Cryst. Solids **354**, 1155–1158 (2008).
51. K. S. Kim, P. J. Bray, and S. Merrin, "Nuclear magnetic resonance studies of the glasses in the system PbO-B_2O_3-SiO_2," J. Chem. Phys. **64**, 4459–4465 (1976).
52. P. W. Wang and L. P. Zhang, "Structural role of lead in lead silicate glasses derived from XPS spectra," J. Non-Cryst. Solids **194**, 129–134 (1996).
53. L. P. Wang, Y. Q. Zhao, S. H. Xu, and M. Y. Peng, "Thermal degradation of ultrabroad bismuth NIR luminescence in bismuth-doped tantalum germanate laser glasses," Opt. Lett. **41**, 1340–1343 (2016).
54. X. Fan, L. Su, G. Ren, X. Jiang, H. Xing, J. Xu, H. Tang, H. Li, L. Zheng, and X. Qian, "Influence of thermal treatment on the near-infrared broadband luminescence of Bi:CsI crystals," Opt. Mater. Express **3**, 400–406 (2013).
55. H. Kogelnik, "Coupled wave theory for thick hologram gratings," Bell Labs Tech. J. **48**, 2909–2947 (1969).
56. Y. Nasu, M. Kohtoku, and Y. Hibino, "Low-loss waveguides written with a femtosecond laser for flexible interconnection in a planar light-wave circuit," Opt. Lett. **30**, 723–725 (2005).